3. Experimental techniques

3.1. Introduction

The experimental configuration to grow the scale as constructed at the University of Pretoria, is similar to the Cahn microbalance (the same equipment as used in the CISR work previously performed by Bahri Ozturk and Arianna Morales). The experimental approach contains the following elements:

- Scale growth under conditions of gas atmosphere, gas flow rate and temperature which simulate reheating conditions, using large samples to avoid edge effects.
- Mechanical descaling of the hot samples
- Assessment of interfacial roughness and the amount of residual scale by examining sample cross-sections by scanning electron microscopy (SEM).

3.2. Experimental set-up (Scale growth)

3.2.1. Gas system set-up

The gas composition was chosen to simulate the combustion product of methane (CH_4) with air, with 3% or 4% excess free oxygen. The total gas flow rate was 4Ndm^3 per minute, which was selected to give similar mass transfer conditions (which depend on the Reynolds number) to industrial furnaces. A schematic representation of the gas system is depicted in figure 9. The gas system contained three separate gas lines for N_2, O_2, and CO_2. The gases used were chemically pure CO_2 (99.0% minimum purity), chemically pure O_2 (99.5% minimum purity) and chemically pure N_2 (99.5% minimum purity). The nitrogen gas was stripped of any excess moisture by passing the gas through a drierite (anhydrous $CaSO_4$) column. The three gas lines were then joined before the gas mixer, after the flow rates had been set.

The gas flow rates were measured and controlled by rotameters, which were calibrated using a bubble-meter. In-line calibration of the rotameters was required to establish the exact flow rate of the gas mixture because a backpressure in the gas line would affect the flow rate.

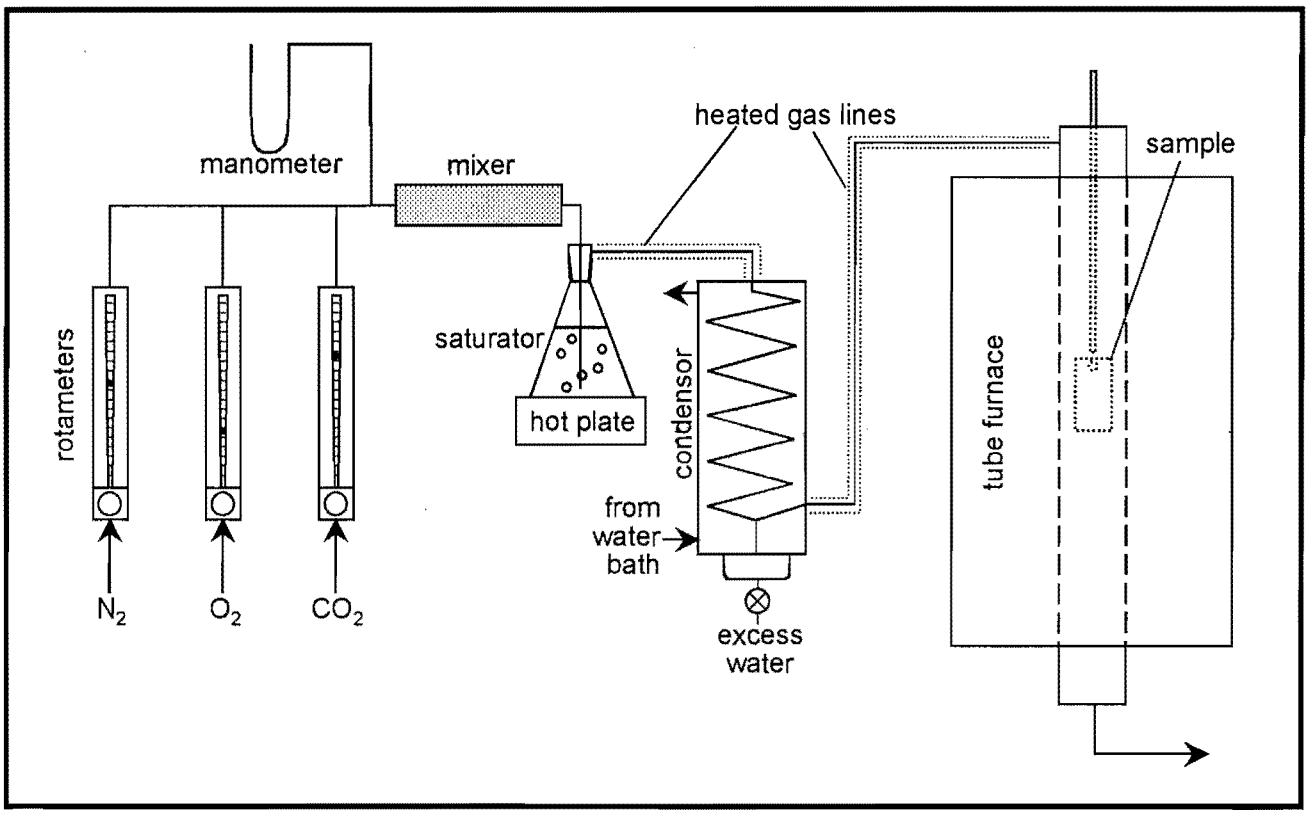

Figure 9 : Experimental configuration used to grow scale under simulated reheating furnace conditions

For this calibration purpose, the outlet from the furnace bottom at the end of the gas system was connected to the bottom of the bubble meter cylinder. The gas was introduced into the bottom of the apparatus, displacing a soap bubble along the length to the top end of the cylinder. A stopwatch was used to establish the time required for one bubble to traverse an indicated volume. The flow rate of the gas was thus calculated by dividing the amount of divisions (cm^3) which the bubble moved by

the time (s) taken for the displacement. This measurement was repeated about six times to establish a good average value for each rotameter setting.

The inlet pressure into the rotameters was measured by a mercury manometer, thus indicating the backpressure relative to the atmosphere. Rotameter corrections for gas density were done since changes in gas density could significantly affect the airflow measurements by rotameters. Using a rotameter at a pressure different than that for which it was calibrated, could yield serious error. The rotameter corrections are shown in detail in appendix 3.

The gas mixer consisted of a glass cylinder filled with glass beads in order to facilitate turbulent flow of the gases through the cylinder for proper mixing of the gases. The gas mixture then entered a saturator — that was basically filled with water kept close to its boiling point. The gas mixture was thus saturated with water vapour. By passing the mixture through a controlled-temperature glass condenser (figure 10), the excess water in the mixture was stripped.

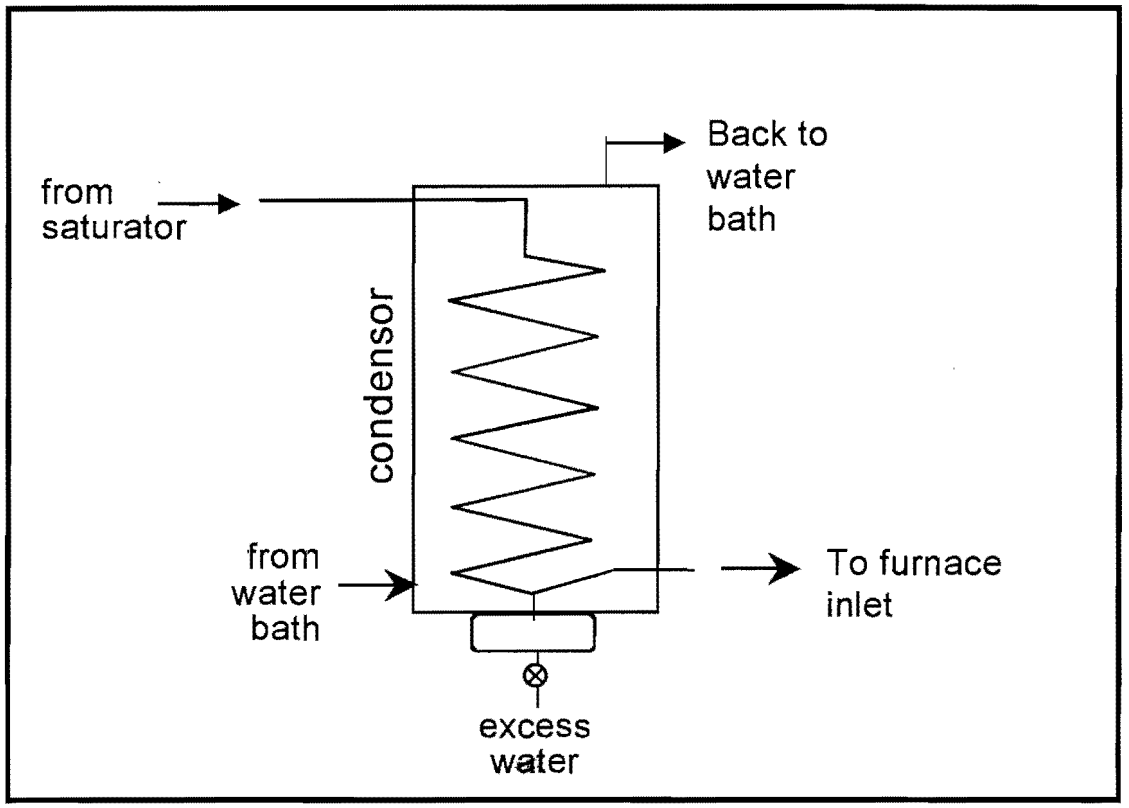

Figure 10 : Figure of temperature-controlled glass condenser

The temperature of the water circulating in the outer section of the condenser was kept at 60 ^{0}C. Control of this temperature was achieved by using a water bath, which was fitted with a pump that enabled the bath to be used as a circulator. The heater power of the bath was 1.4 kW, with a stability of approximately 0.1 ^{0}C. To ensure that any excess vapour in the mixture would condense, the mixture exited the condenser at angle and was fed into the furnace. A three-way brass valve was fitted between the condenser exit and the furnace inlet. A heavy insulated heating tape with a knitted heavy Fibrox fabric covering (Barnstead Thermolyne) was used to heat all the connections between the water saturator and the furnace. The variable transformer controlling the heating tape temperature was set at 135V to ensure that the temperature of the heating tape was approximately 80 ^{0}C.

Silicon rubber tubing was used for all the connections between the regulators and the glass-condenser. PFA- tubing (Swagelok) was used for the connections between the

three-way valve and the furnace simply because the hardness of the tubing made wrapping the heating tape around it easier.

The gas system was checked for leaks by filling the gas system with He and checking for leaks with a He-detector, one section at a time.

3.2.1.1 REQUIRED GAS FLOW RATES IN FURNACE

The specimen size and furnace bore diameter, were used to fix the minimum required gas flow rate through the furnace, to ensure that oxygen mass transfer to the scale surface was sufficient to yield the required oxidation rate. The results of calculations of the required gas flow rate are presented below, to show that these can be feasibly obtained in the large-bore tube furnace. The calculations were based on the combustion product of methane with air, to yield a product gas containing 3% excess oxygen; the other components of the gas were calculated by a mass balance to be 73% N_2, 16% H_2O and 8% CO_2. The report of Abuluwefa, *et al.* (1996) indicates that the initial rate of mass gain of the carbon steel samples during reheating at 1200°C is 1.7×10^{-4} kg/m^{2}s. The required oxygen mass transfer constant to match this rate is defined by the expression for the mass-transfer-controlled reaction:

$$K = m_{O_2}(C_{O_2}^{g} - C_{O_2}^{int}) \qquad (1)$$

Where K is the rate of mass gain (in kg/m^{2}s), m_{O_2} is the mass transfer constant of oxygen in the gas phase (in m/s), and C_{O_2} is the concentration of oxygen (in kg/m^3), where the superscripts "g" and "int" refer to the gas stream and the gas-scale interface respectively. Assuming $C_{O_2}^{g} >> C_{O_2}^{int}$, and taking $C_{O_2}^{g} = 6.7 \times 10^{-3}$ kg/m^3 (valid for a 3% oxygen mixture, at the typical reheating temperature of 1500 K, and atmospheric pressure of 0.865 atm), the required mass transfer constant of oxygen is calculated to be m_{O_2}=0.025m/s. This mass transfer constant is obtained by controlling the gas flow rate to yield the appropriate Reynolds number, as shown by the expression below (Abuluwefa, *et al,* 1996):

$$m_{O_2} = (4D_{O_2}/3L)\,(Re)^{1/2}(Sc)^{1/3} \qquad (2)$$

Where D_{O_2} is the diffusion coefficient of oxygen in the gas mixture (taken to be 3.27×10^{-4} m^2/s [Turkdogan, 1980]), L is the sample length (0.1m), Re is the Reynolds number (uL/ν), and Sc is the Schmidt number (ν/ D_{O_2}); u is the gas velocity and ν is the kinematic viscosity of the gas. Taking the viscosity of the gas to be $\nu = 2.3\times10^{-4} m^2/s$ (Turkdogan, 1980), the required Reynolds number was calculated to be 41.7, yielding a required gas velocity of 0.10m/s, or a gas flow rate of $8.3\times10^{-5} Nm^3/s$. This means that the required flow rates of nitrogen, carbon dioxide and oxygen are respectively $3.59 Ndm^3/min$, $0.4 Ndm^3/min$, and $0.15 Ndm^3/min$. After calibration and correction of the rotameters for gas density, the actual flow rates of nitrogen, carbon dioxide and oxygen that were used were respectively $3.91 Ndm^3/min$, $0.44\ Ndm^3/min$, and $0.16\ Ndm^3/min$ (appendix 3).

3.2.2. Furnace set-up

The experiments were carried out in a vertical tubular furnace consisting of a pure (99.8% purity) mullite process tube with an inside diameter of 7.6 cm allowing samples of 5 cm width and 10 cm length to be oxidized. A schematic representation of the furnace assembly is shown in figure 11.

The maximum temperature that could reliably be reached in the available laboratory furnace without drastically reducing the life of the elements was 1400 ^0C. The furnace temperature was controlled by a Eurotherm 902P controller / programmer using a thermocouple that was positioned next to the furnace tube, close to the hot zone.

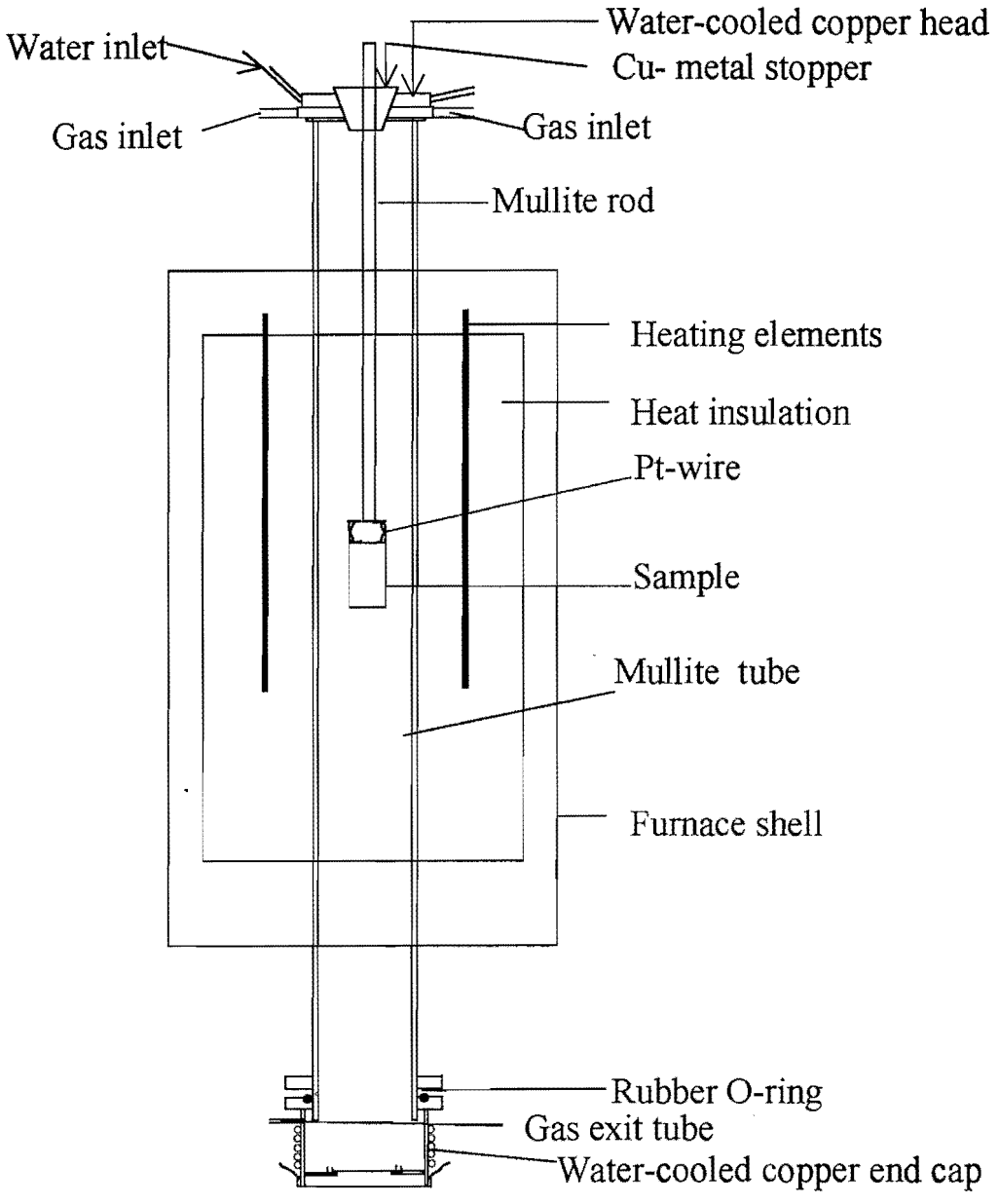

Figure 11 : Schematic representation of furnace assembly

The exact position of the hot zone in the furnace was measured by placing a hand-held K-type (Ni-Cr) thermocouple at various depths into the furnace tube. The

temperature profile as a function of position at a programmed temperature of 1250 ^{0}C is shown in figure 12. The reference point from which the depth was measured was the furnace top.

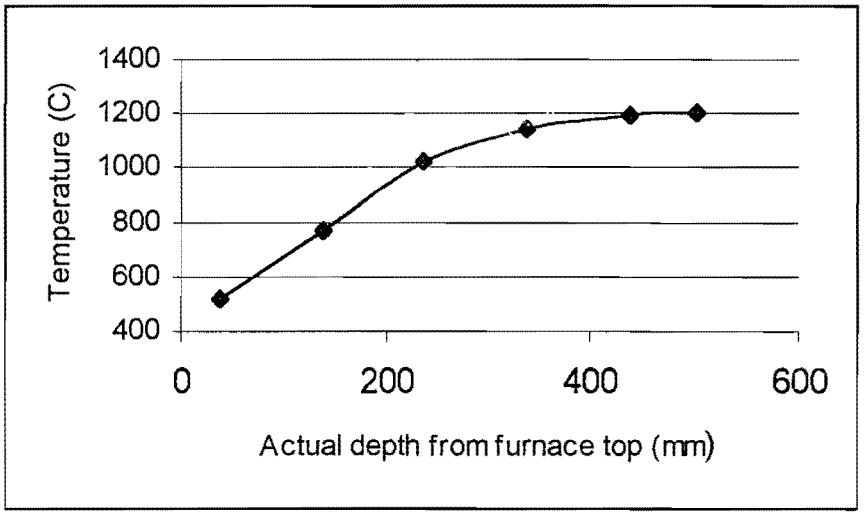

Figure 12 : Temperature profile as a function of position. (Depth measured from top of furnace. Programmed furnace temperature: 1250 ^{0}C. The average measured temperature in the hot zone was approximately 1200 ^{0}C.

The average temperature of the hot zone measured with the hand-held thermocouple was within 40 ^{0}C of that indicated by the furnace controller as shown in figure 13 below. This correlation was used to program the furnace temperature accurately.

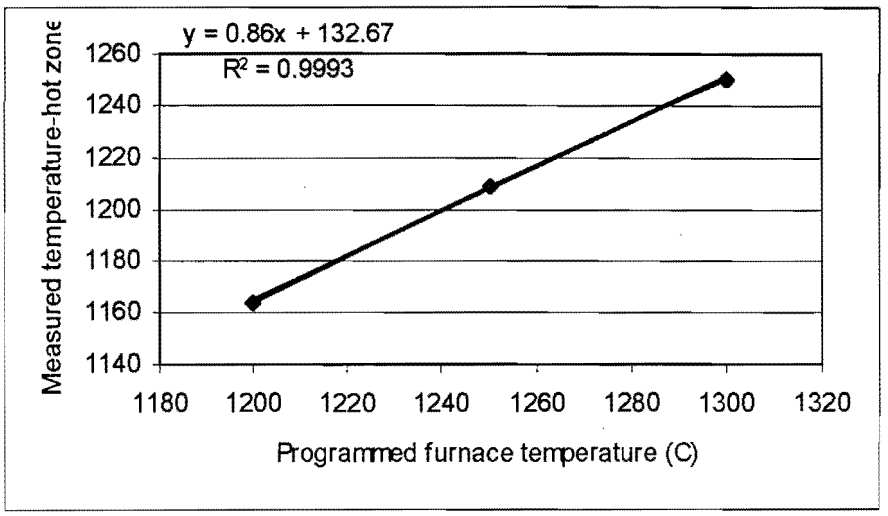

Figure 13 : Measured temperature in hot zone versus programmed furnace temperature at a depth of 503 mm below furnace top

The mullite furnace tube (90 mm O.D. x 76 mm I.D. x 1500 mm length) was fitted with water-cooled copper heads at both ends. The bottom fitting extended below the mullite tube and was sealed with an O-ring lubricated with high temperature vacuum grease. The upper end cap was sealed to the open flat end of the tube, sealing into a rubber gasket between the tube and the fitting. A steel bracket attached to the furnace tube exerted pressure on the gasket. Within the furnace, the sample was suspended from a mullite rod (8 mm I.D. and 1000 mm length) by means of platinum wire.

PVC - braided tubing was used for connecting the cooling water inlet and outlet to the furnace. Quick-connect couplings were used to ensure that the cooling water tubes could easily be removed from the copper-end cap before descaling of the sample.

3.3. Experimental set-up (Descaling)

At the end of the scaling period, the sample was removed from the furnace and subjected to mechanical descaling whilst hot. Literature observations indicated that the action of hydraulic descalers was largely mechanical (section 2). This meant that a mechanical means of descaling at temperature should yield an adequate simulation of in-plant hydraulic descaling. Thus, the mechanical descaling method of Tuck and Barlow (1972) was used, namely transferring the sample from the furnace to a bending rig. The rig used for this purpose is illustrated in Figure 14. As indicated the hot sample is placed on a U-shaped tool steel anvil, and then bent by a tool steel punch pressing on the center of the sample. The total time from opening of the furnace to deformation of the sample is about 30 seconds. The punch is driven by a pneumatic cylinder, which can give a maximum force of 10 kN (the calculation is shown below). The vertical displacement of the hammer is controlled by means of limit switches to ensure that the amount of deformation is the same in each case (to yield the same radius of curvature). The force required to deform the specimen was estimated from the expression for fully plastic bending of a beam (Hosford, *et al,* 1983):

$$F = \frac{bd^2\sigma}{L} \tag{3}$$

Where b, d and L are the sample width, thickness, and length respectively, and σ is the yield stress. Taking σ =50 MPa (Metals Handbook, 1980), b= 0.05m, d= 0.01m and L= 0.1m, the required force is calculated to be 2.5 kN, which is well within the capability of the available pneumatic cylinder, using compressed air available in the laboratory.

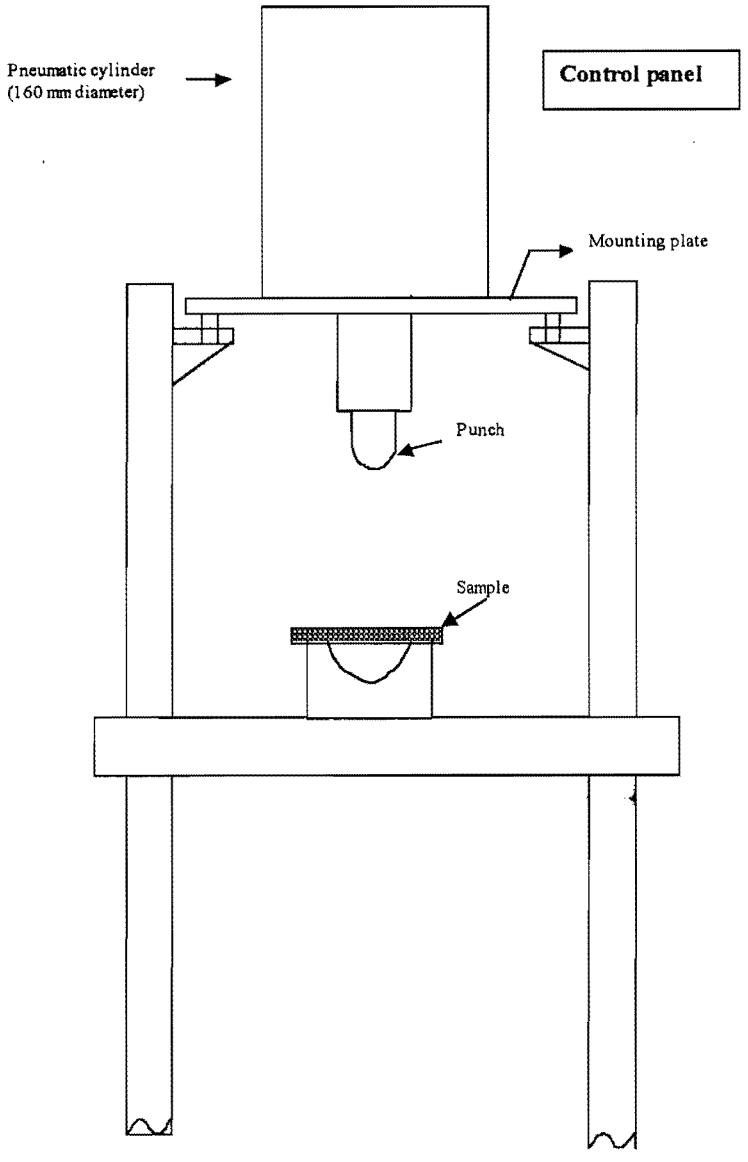

Figure 14 : Schematic representation of bending rig, to yield mechanical descaling

The validity of this method was assessed by testing whether it yielded the same descalability ranking as that observed in industry (e.g. comparing 11.5% chromium steel and type 304, and different amounts of excess oxygen.)

Figure 15 gives a closer view of the punch and anvil combination used to give mechanical descaling. The dot-dash lines show the position of the sample.

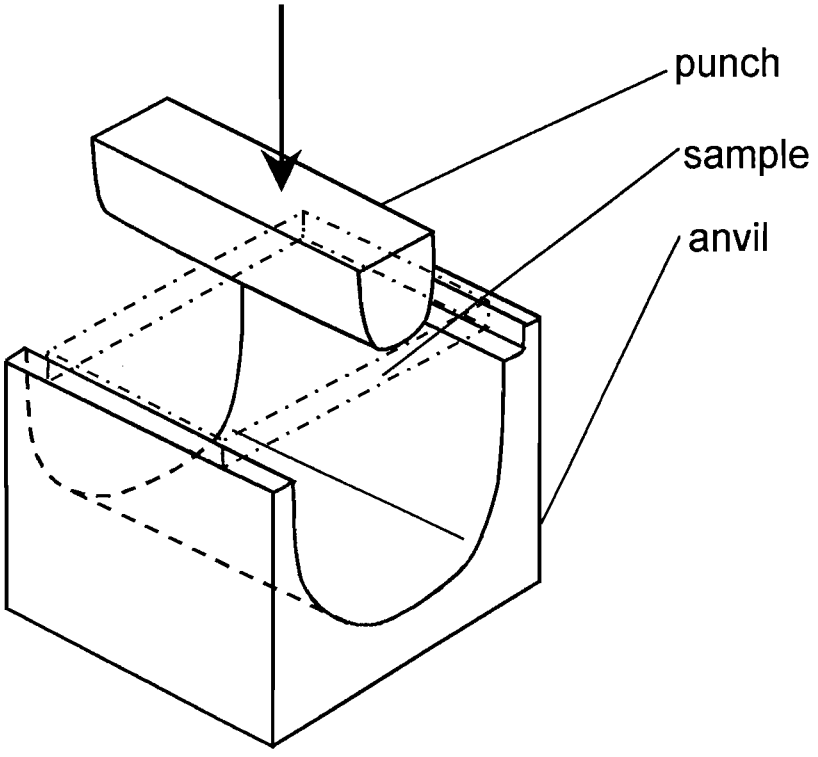

Figure 15 : Punch-and-anvil combination used to give mechanical descaling

Transfer of the samples from the furnace to the descaling station had to be performed in a standardized way, since cooling of the surface before descaling is detrimental to scale removal (Sheppard, and Steen, 1970). The interfacial roughness and the amount of residual scale were assessed by examining sample cross-sections by scanning electron microscopy (SEM). The calculations are shown in detail in appendix 6.

3.4. Experimental procedure

3.4.1. Sample size and preparation

Given the expected strong effect of steel compositions (nominal composition and impurity content) different grades of steel were used to test these effects. Since the 11.5% chromium stainless steel is said to behave very differently from type 304, these two stainless steels were considered in this study. Thus the steels used were samples of type 412 and 304 stainless steel. Samples from different heats of the two steel grades were used in this work. However, these were similar in chemistry and microstructure, and average chemical compositions are given in the table below.

Element	Grade	
	412	304
C	0.021	0.044
S	0.0024	0.0033
P	0.026	0.022
Mn	0.485	1.305
Si	0.72	0.40
V	0.08	0.12
Cu	0.09	0.09
Co	0.02	0.03
Ti	0.034	0.010
Mo	0.02	0.14
Cr	11.62	18.16
Ni	0.34	8.09
Al	0.002	0.004
Nb	0.002	0.003
B	0.003	0.001
N	0.0213	0.050
O	0.0037	0.0080

Figure 16 : Table of chemical compositions (mass percentages) of samples

The samples were cut to size from hot-rolled plate using a band saw as well as a fixed abrasive disc cutter. The samples were typically around 100 mm x 50 mm x 10

mm large. 3 mm holes – through which Pt-wire was passed to hang the sample - were drilled close to one of the shorter sides of the sample. These comparatively large sample dimensions were required to minimize the relative effects of scale growth stresses at the specimen edges and corners; the principle is to have the width and length large compared with the scale thickness (which could approach 5 mm for long reheating times). If smaller specimens were used, the growth stresses (which inevitably arise during oxide growth) could detach the scale from the steel surface, so altering the scale growth rate and adhesion.

The stainless steel samples used here had been pickled clean in the plant, and were hence only degreased (with acetone) before scaling.

3.4.2. Experimental run

As mentioned earlier, the gas composition was chosen to correspond to the combustion products of methane with air, with 3% or 4% excess oxygen. The total gas flow rate was 4 Ndm^3/min. To ensure that the gas composition was correct the gas mixture was analyzed regularly using a Gaslab 300 gas analyzer (appendix 4). Thus the gas composition was obtained by mixing the nitrogen, oxygen and carbon dioxide in a glass bead mixer and saturating this with water vapour by passing the mixture through water kept near its boiling point (as discussed in paragraph 4.2.1.1). The mixture was then fed into the furnace.

Some preliminary experiments were done to ensure that the correct amount of water vapour entered the furnace. This was done by passing the exit gas at the bottom of the furnace through a drierite column that had been pre-weighed. After the experiment the drierite column was then weighed again. The difference between the two weights, gave the amount of water that had been absorbed by the drierite. This value was then compared to the theoretically calculated mass of water that was

expected to be in the gas mixture. In all of the experiments the values were quite similar (appendix 4).

At the end of the scaling period, the sample was removed from the furnace and subjected to mechanical descaling whilst hot. Following mechanical descaling and cooling of the sample (in air for stainless steel, with the sample placed on a stainless steel plate which acts as a heat sink), samples were cut from the region of tensile deformation and from the undeformed region of the sample (as illustrated in figure 17), using a band saw.

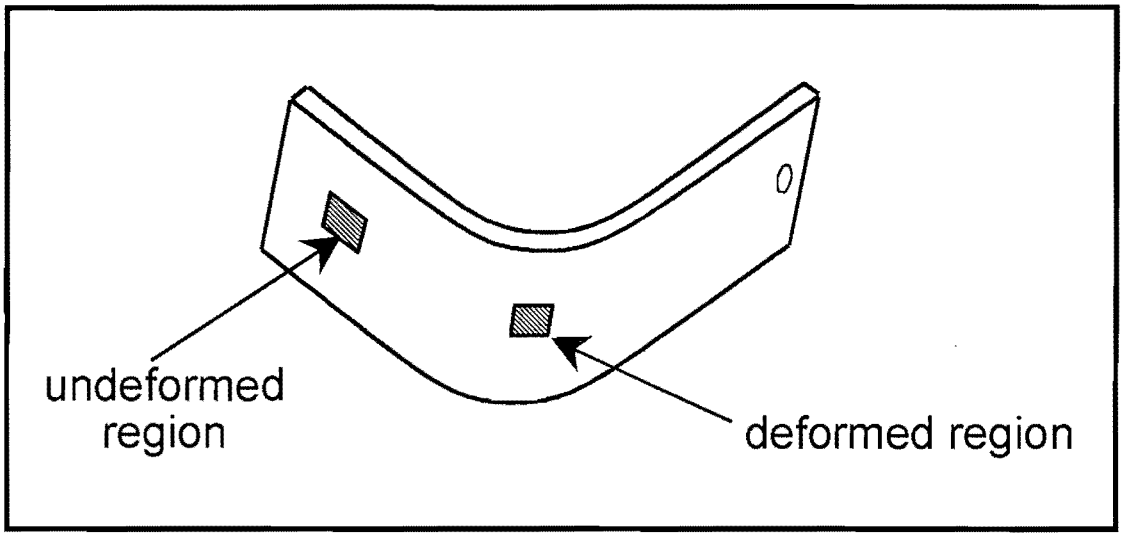

Figure 17 : Location of samples to assess the degree of descaling, within the reheated sample which had been descaled by bending

The samples were mounted in metallographic resin, machined away and then polished to allow a cross-section near the center of the sample to be examined (so avoiding possible edge effects). The samples were examined in a scanning electron microscope (recording the secondary electron image). Backscatter electron imaging (at an acceleration voltage of 15 kV) was used to show the nature of the scale-steel interface. Energy-dispersive X-ray analysis (EDX) was used for point analyses of the

various phases. The average thickness of scale remaining on the descaled surfaces was found by means of image analysis (of the SEM images).

The basic matrix of experiments done is shown in the table below.

Temperature (^{0}C)	% O_2	Reheating time(hr)
1280	3	1.5
1250	4	3
		6

Figure 18 : Experimental matrix for type 304 stainless steels

For the type 304 stainless steels some preliminary experiments were done at a reheating temperature of 1245 ^{0}C. These experiments served to test whether the experimental configuration as assembled, could be used successfully to simulate scale growth and descaling. The type 304 steel was used in this initial assessment, both because of ready availability of suitable plate material and because of the apparent contradiction between the observation of substantial steel-scale entanglement and the plant observation of good descalability (which hence made this a good test for the validity of the laboratory test).

In the next batch of experiments done, all the samples were reheated isothermally at 1280 ^{0}C and 1250 ^{0}C, with free oxygen contents in the gas stream of 3 % and 4 % oxygen respectively, and reheating times ranging from 1.5 hours to 6 hours. The reheating temperature of 1250 ^{0}C is similar to the actual reheating temperature of type 304 stainless steels in industry. A few preliminary experiments were also done at reheating temperatures of 1230 ^{0}C and 1260 ^{0}C.

For the type 412 stainless steels, all the samples were also reheated isothermally at 1280 ^{0}C as well as 1210 ^{0}C, with free oxygen contents in the gas stream of 3 % and 4 % oxygen respectively, and reheating times ranging from 1.5 hours to 6 hours. The reheating temperature of 1210 ^{0}C is similar to the actual reheating temperature of type 412 stainless steels in industry.

Temperature (^{0}C)	% O_2	Reheating time(hr)
1280	3	1.5
1210	4	3
		6

Figure 19 : Experimental matrix for type 412 stainless steels

The temperature during reheating was generally monitored and controlled by means of the furnace thermocouple. However in two runs an additional (R-type) thermocouple was spot-welded to the sample surface to ensure more careful measurement of the sample temperature in the furnace. Since the gas which is introduced into the furnace is not preheated, this will tend to quench the sample slightly, whereas the exothermic nature of the scaling reaction tends to conversely heat the sample surface to a slightly higher temperature than the furnace hot zone.

The furnace temperature used for these experiments was 1280 ^{0}C, in an atmosphere with 3% excess oxygen. The samples were reheated for approximately 3.5 hours. The recorded sample temperatures were plotted in the graphs below.

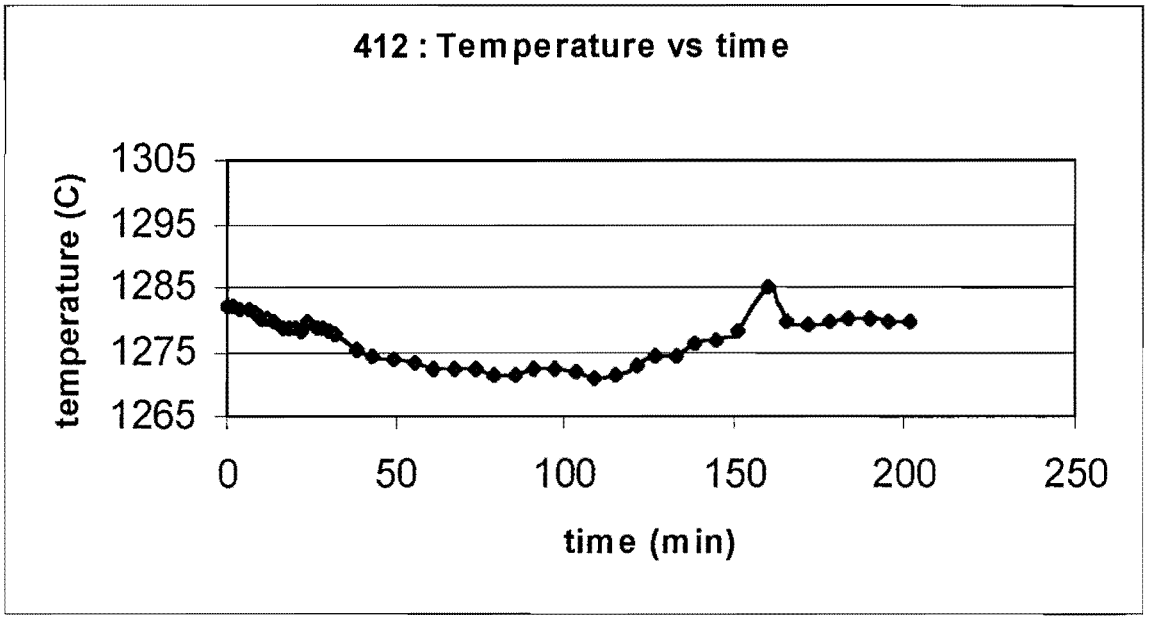

Figure 20 : Type 412-sample temperature as a function of time

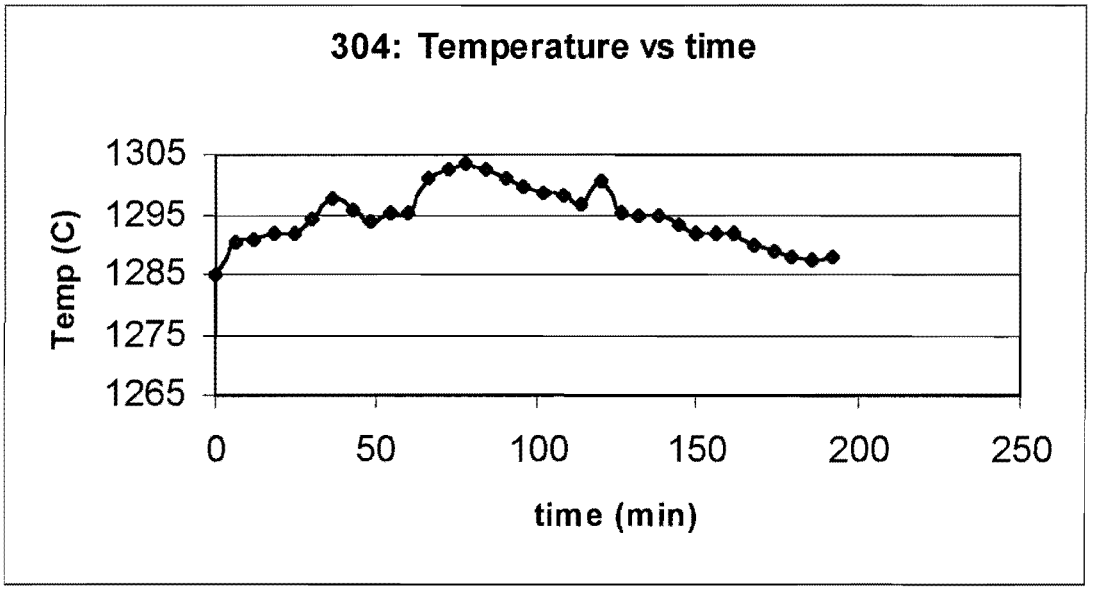

Figure 21 : Type 304-sample temperature as a function of time

It was found that the sample temperature was generally within 10 ^{0}C of the furnace temperature (1280 ^{0}C). Thus the samples did not heat significantly above the furnace temperature. Although some heating was expected from the exothermic nature of the oxidation reactions, it was found that this was not significant for these samples.

4. Results

4.1. Stainless steel type 412

The scale had a complex structure. The outer layer was iron oxide containing little or no chromium. The inner layer of scale largely consisted of an iron-chromium spinel, but with more phases present close to the interface with the steel. Closer examination of the metal-scale interface revealed severe entanglement at the interface.

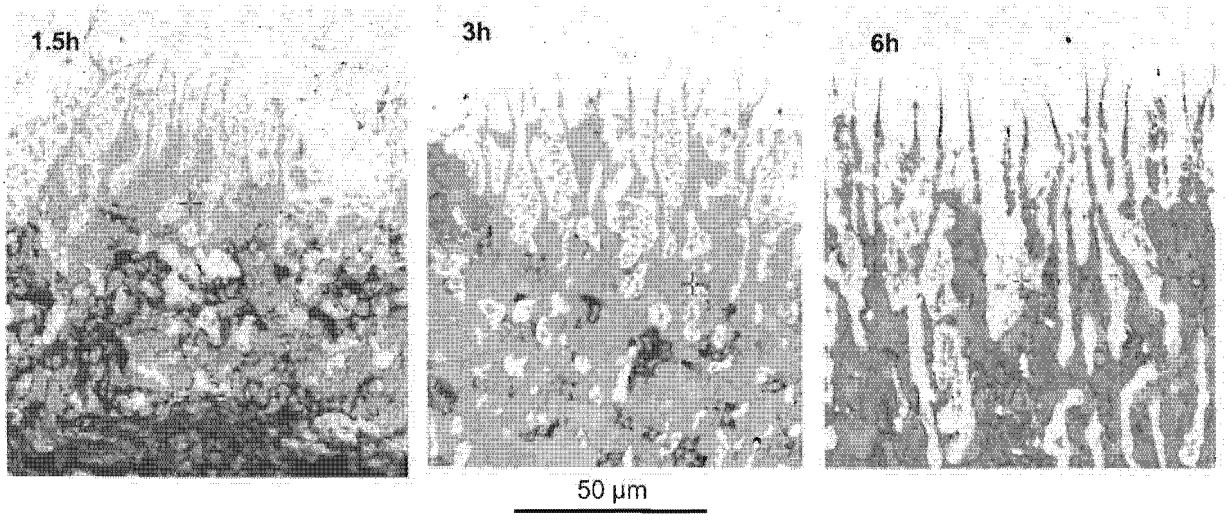

Figure 22 : Scanning electron micrographs of the scale-steel interface of type 412 samples held at 1210 ^{0}C with 4% excess O_2 for different holding times (as indicated on the micrographs).

The metal is at the top of the images in figure 22 and the scale at the bottom. The width of the entangled zone appears to increase as the holding time increases and the tendrils of metal become much coarser. These coarser tendrils perhaps anchor the scale more strongly to the steel, with the resulting poorer descaling. Given that interfacial roughening arises in this steel but is not reported in literature for (pure)

binary iron-chromium alloys, the residual elements must play a role. Closer examination of the entangled region reveals an effect of silicon. As the table of steel compositions (figure 16) indicates, the steel contains 0.72% Si. This silicon (once oxidised) accumulates at the scale-metal interface and forms a fayalite melt.

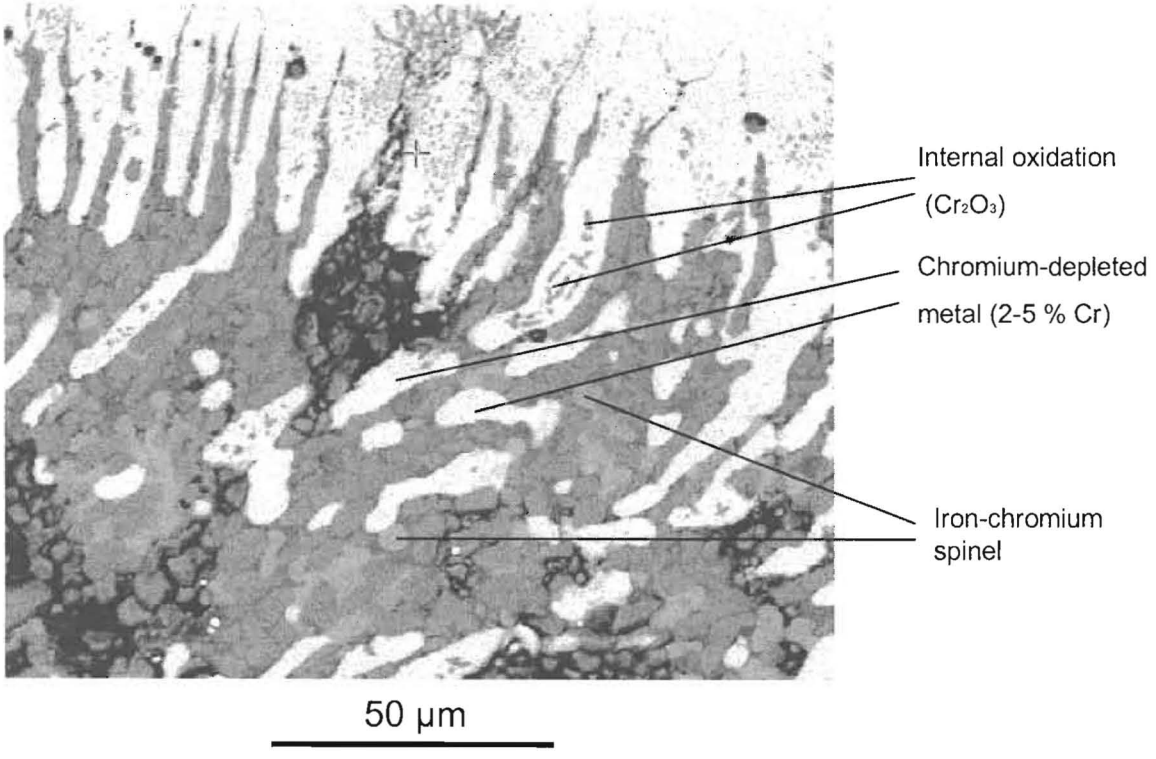

Figure 23 : Detail of the structure in the entangled region, showing internal oxidation

The metal at the interface is chromium-depleted as shown in figure 23. The metal contains approximately 2-5 % chromium as indicated by the point analyses in appendix 5. This low chromium content is the result of precipitation – by internal oxidation – of Cr_2O_3 within the metal. Upon oxidation of the remaining iron to iron oxide the Cr_2O_3 is converted to the spinel scale, and some iron is transported through the spinel scale to precipitate as the iron oxide scale at the outer surface. This sequence of phases is as expected from the iron-chromium-oxygen phase diagram (Laheij et al, 1980).

4.1.1. Residual scale thickness

4.1.1.1 REHEATING TEMPERATURE : 1210 ^{0}C

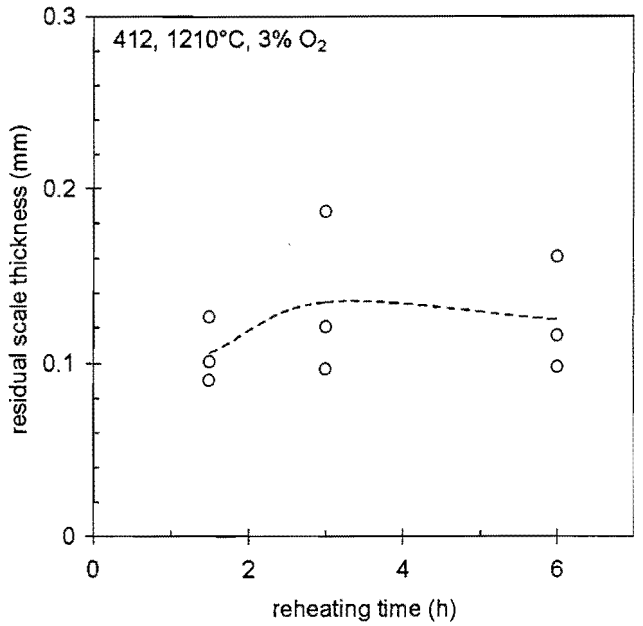

a)

Type 412, at 1210 ^{0}C with 3% O_2

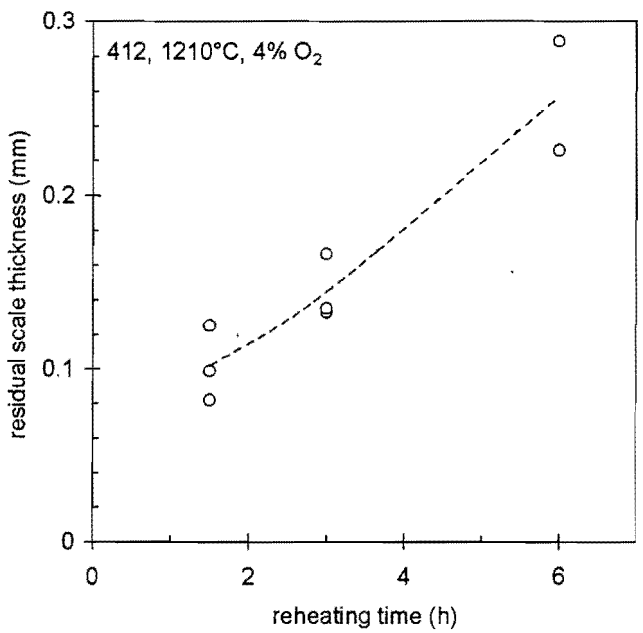

b)

Type 412, at 1210 ^{0}C with 4% O_2

Figure 24 : Measured residual scale thickness for type 412 samples, reheated at 1210 ^{0}C, for varying times and with 3% and 4% oxygen in the furnace atmosphere

The graphs on the previous page show the measured residual scale thicknesses, for type 412 samples that were reheated at 1210 ^{0}C, for varying reheating times and with 3% and 4% oxygen in the furnace atmosphere. The data points show measurements at three positions on each descaled surface and the broken line the average of these measurements. The results show that the 412 steel grade is quite sensitive to reheating time and excess oxygen, with increases in both elevating the amount of residual scale.

The following graphs below (figure 25) illustrate the way in which the width of the entangled region increases with longer reheating times and higher excess oxygen contents, for type 412 stainless steel. This is in line with the effect of such processing changes on the amount of residual scale (figure 24).

The micrographs in figure 22 differ from those in figure 25 (for 4% excess oxygen) because in figure 22 the micrographs were taken from the undescaled section of the sample (concave part of the deformed region in figure 17), whilst in figure 25 the micrographs were from the descaled section of the sample (convex part of the deformed region in figure 17).

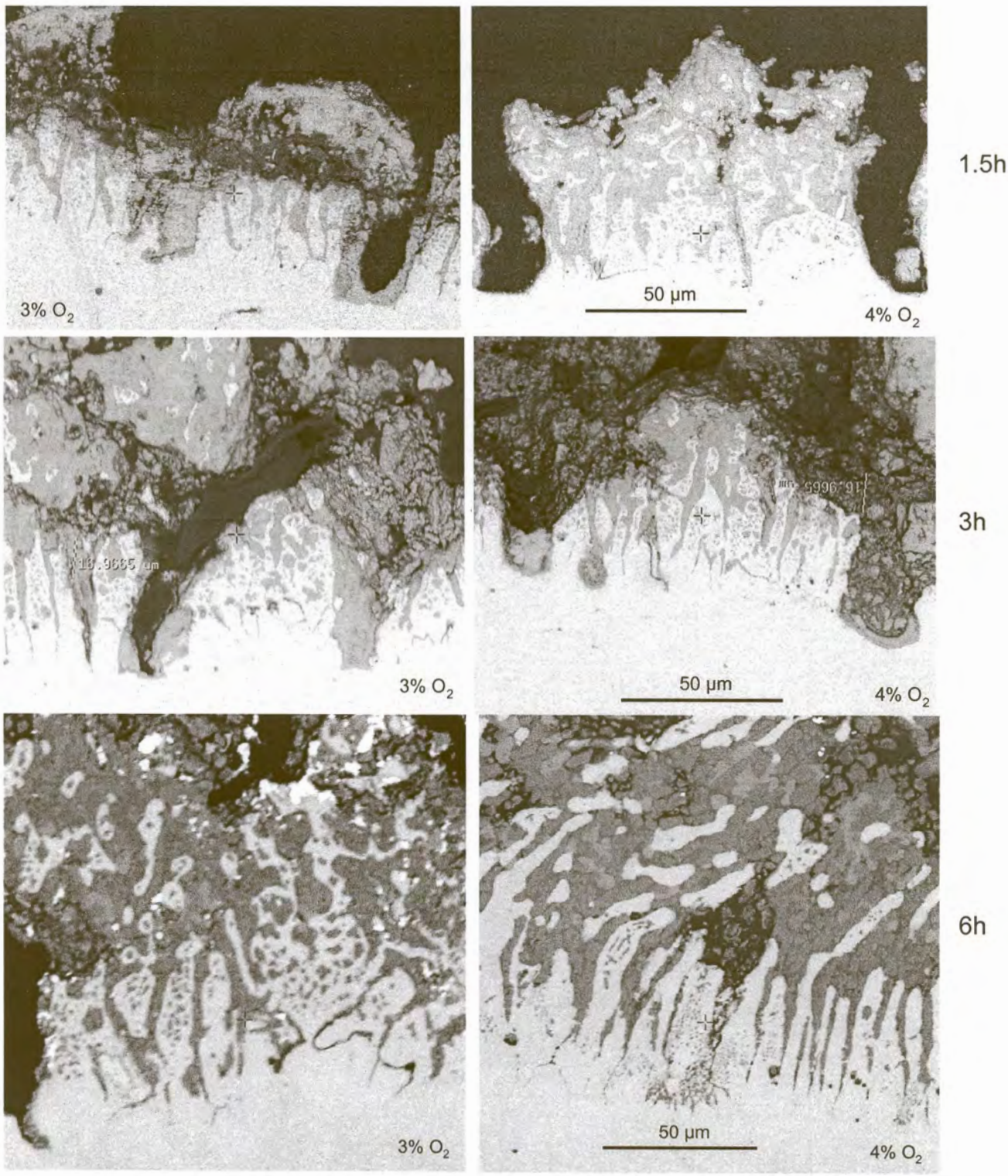

Figure 25 : Development of entanglement at the scale-steel interface, for type 412 steel at a reheating temperature of 1210 ^{0}C (scanning electron micrographs)

In all of the images, the scale is towards the upper part of the image and the steel substrate towards the bottom. All the samples were mechanically descaled. Each pair of images is for the same reheating time, but for two different levels of excess oxygen.

The direct link between the width of the entangled region and the residual scale thickness is illustrated by figure 26, which shows a lower magnification image of a sample, which had been reheated for 6 hours and then mechanically descaled. Evidently fracture of the scale occurred at the edge of the entangled region, leaving the entire entangled region attached to the substrate. The strong effect of reheating conditions on the amount of residual scale has clear implications for the need to control excess oxygen closely in industrial operations.

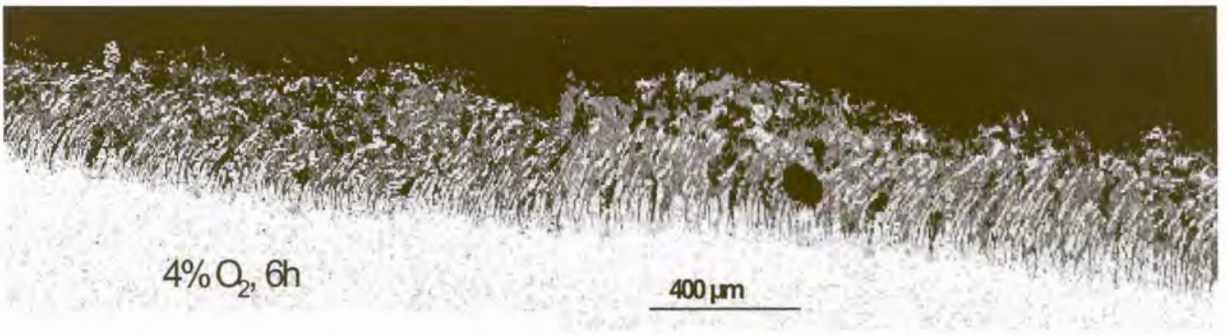

Figure 26 : Montage of descaled surface of type 412 sample (reheated at 1210 ^{0}C), showing that the residual scale thickness corresponds to the full thickness of the entangled region

4.1.1.2 REHEATING TEMPERATURE : 1280 ^{O}C

The figures below are for the same conditions as in the previous section however; the reheating temperature is 1280 ^{0}C.

Figure 27 also shows the measured residual scale thicknesses, for type 412 samples. The results also illustrate the sensitivity of the 412 steel grade to reheating time and excess oxygen. However the effect is not similar to the reheating temperature of 1210 ^{0}C and the fact that the residual scale thickness seems to decrease for longer reheating times in figure 27, is quite odd. In both cases of reheating time and excess oxygen at 1280 ^{0}C however, there is still more than 0.1mm scale remaining after 6 hours. The way in which the width of the entangled region develops with longer reheating times and higher excess oxygen contents, for type 412 stainless steel at this higher reheating temperature, is shown in figure 28. In all of the images, the scale is towards the upper part of the image and the steel substrate towards the bottom.

a)

Type 412, at 1280 ^{0}C with 3% O_2

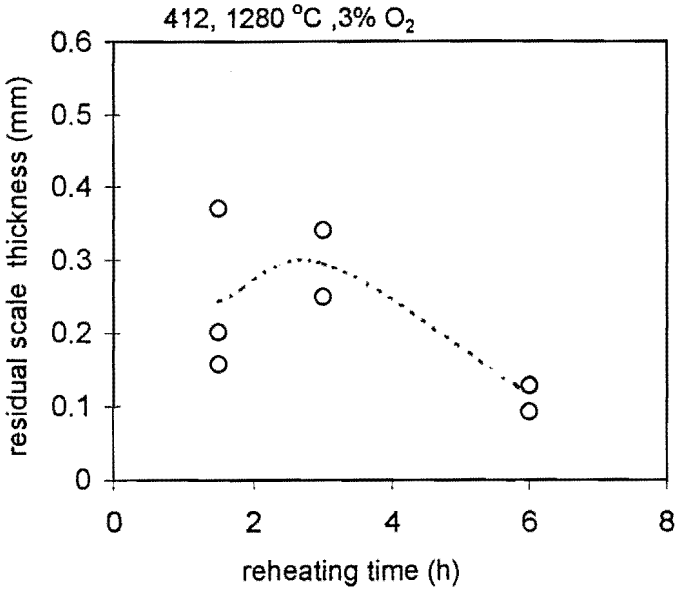

b)

Type 412, at 1280 ^{0}C with 4% O_2

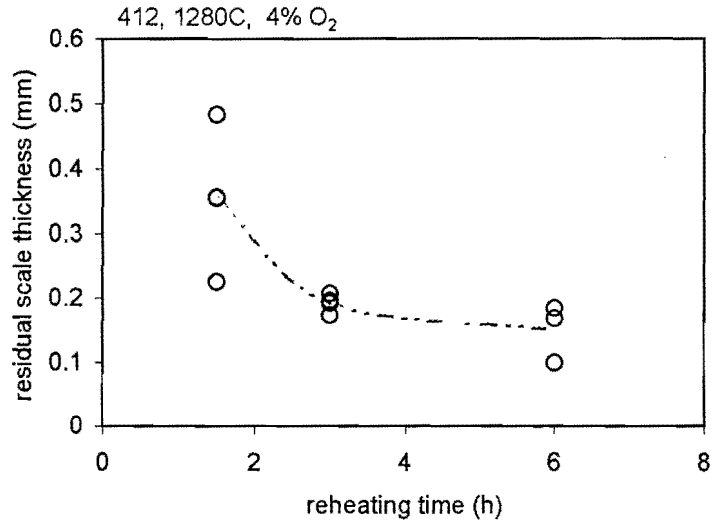

Figure 27 : Measured residual scale thickness for type 412 samples, reheated at 1280 ^{0}C, for varying times and with 3% and 4% oxygen in the furnace atmosphere

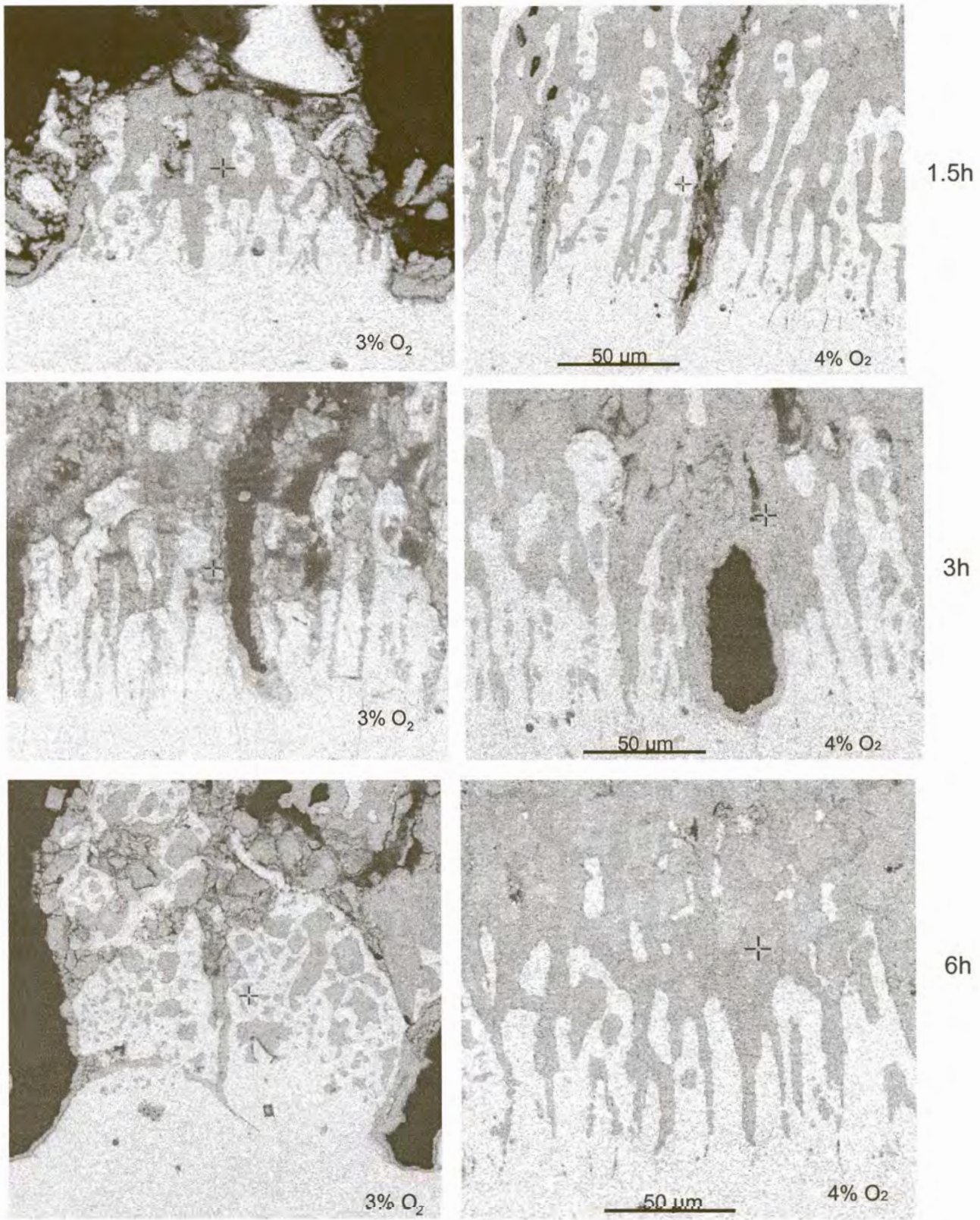

Figure 28 : Development of entanglement at the scale-steel interface, for type 412 steel at a reheating temperature of 1280 ° C (scanning electron micrographs)

Figure 29 shows a lower magnification image of a sample, which had been reheated for 1.5 hours and then mechanically descaled. Fracture of the scale occurred at the edge of the entangled region, leaving the entire entangled region, attached to the substrate. The direct link between the width of the entangled region and the residual scale thickness is illustrated.

Figure 29 : Montage of descaled surface of type 412 sample (reheated at 1280 ^{0}C)

4.2. Stainless steel type 304

Tendrils of unoxidized metal were detected in the scale on the type 304 samples as shown in figure 30. The scale is at the top of the images and the metal at the bottom. The composition (mass percentages) of these tendrils was 4-11% chromium and 12-15% nickel (balance iron) close to the steel-scale interface, with the chromium content decreasing to 3 –4% as you move away from the interface into the entangled scale (appendix 5). Thus at the interface, the composition of the metal tendrils is a chromium-depleted form of the original composition (18.16 % Cr and 8.09 % Ni – as given in figure 16) and nickel enrichment is found in the tendrils which are present in the outer layers of the scale.

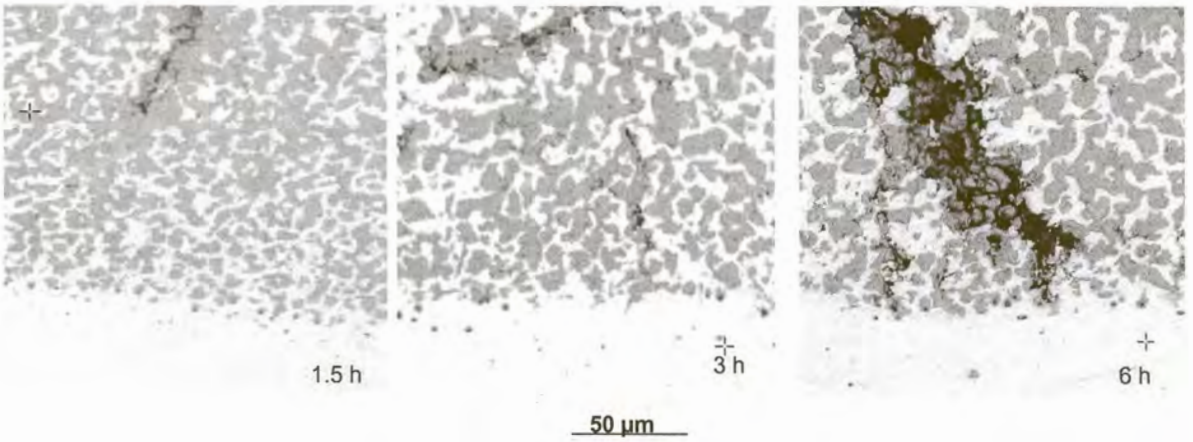

Figure 30 : Scanning electron micrographs of the scale-steel interface region of type 304 samples held at 1280 ^{0}C and 4% excess O_2 for different times (as indicated on the micrographs).

4.2.1. Residual scale thickness

4.2.1.1 REHEATING TEMPERATURE: 1250 ^{O}C

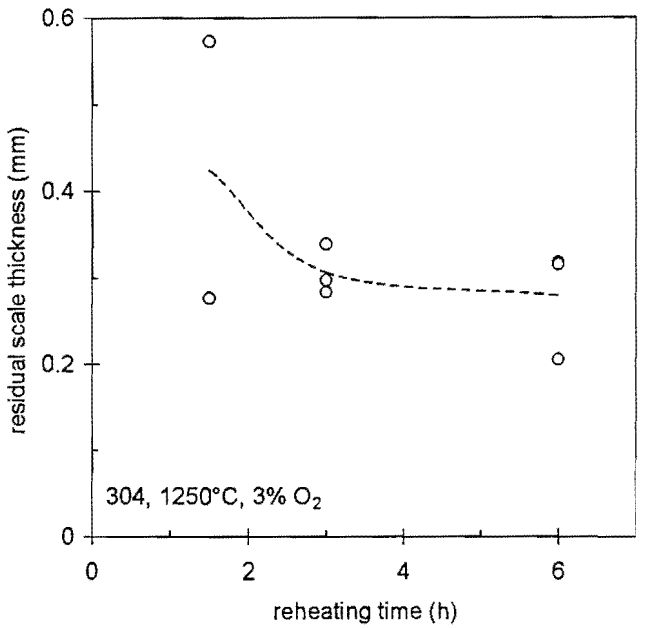

c)

Type 304, at 1250 ^{0}C, with 3% O_2

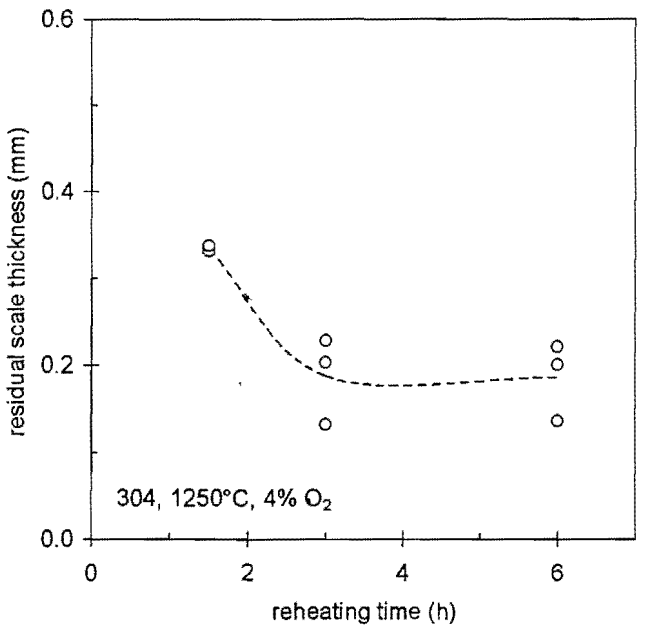

d)

Type 304, at 1250 ^{0}C, with 4% O_2

Figure 31 : Measured residual scale thickness for type 304 samples, reheated at 1250 ^{0}C, for varying times and with 3% and 4% oxygen in the furnace atmosphere

The graphs on the previous page (figure 31) show the measured residual scale thicknesses, for type 304 samples that were reheated at 1250 ^{0}C, for varying reheating times and with 3% and 4% oxygen in the furnace atmosphere. The data points show measurements at three positions on each descaled surface and the broken line the average of these measurements. The residual scale on the type 304 samples at this temperature, were not much affected by reheating conditions; if anything the scale somewhat decreased in thickness for higher excess oxygen and longer reheating. This difference is caused by the way in which the type 304 samples descaled. As figure 32 below illustrates, descaling arose by the formation of numerous cracks through the scale. In all of the images, the scale is towards the upper part of the image and the steel substrate towards the bottom. Each pair of images is for the same reheating time, but for two different levels of excess oxygen.

Closer examination revealed that these cracks followed areas of metal-free scale, as shown at higher magnification in figure 33. ("Metal-free scale" here indicates regions of the scale which consisted of oxide only, without any nickel-enriched metal tendrils). The metal-free chromite scale regions offer low-toughness fracture paths, and hence the extent of descaling is linked directly to the prevalence of these fracture paths in the strongly entangled scale. No descaling was observed between the substrate and the scale where such chromite paths were absent. The chromite layers apparently form by internal oxidation (as indicated by the chromite layer extending into the substrate in the 1.5 hour sample of figure 33), with internal oxidation somewhat more prevalent on the austenite grain boundaries. Hence the location of the chromite layers in the scale (the fracture paths during subsequent descaling) depends on the austenite grain structure.

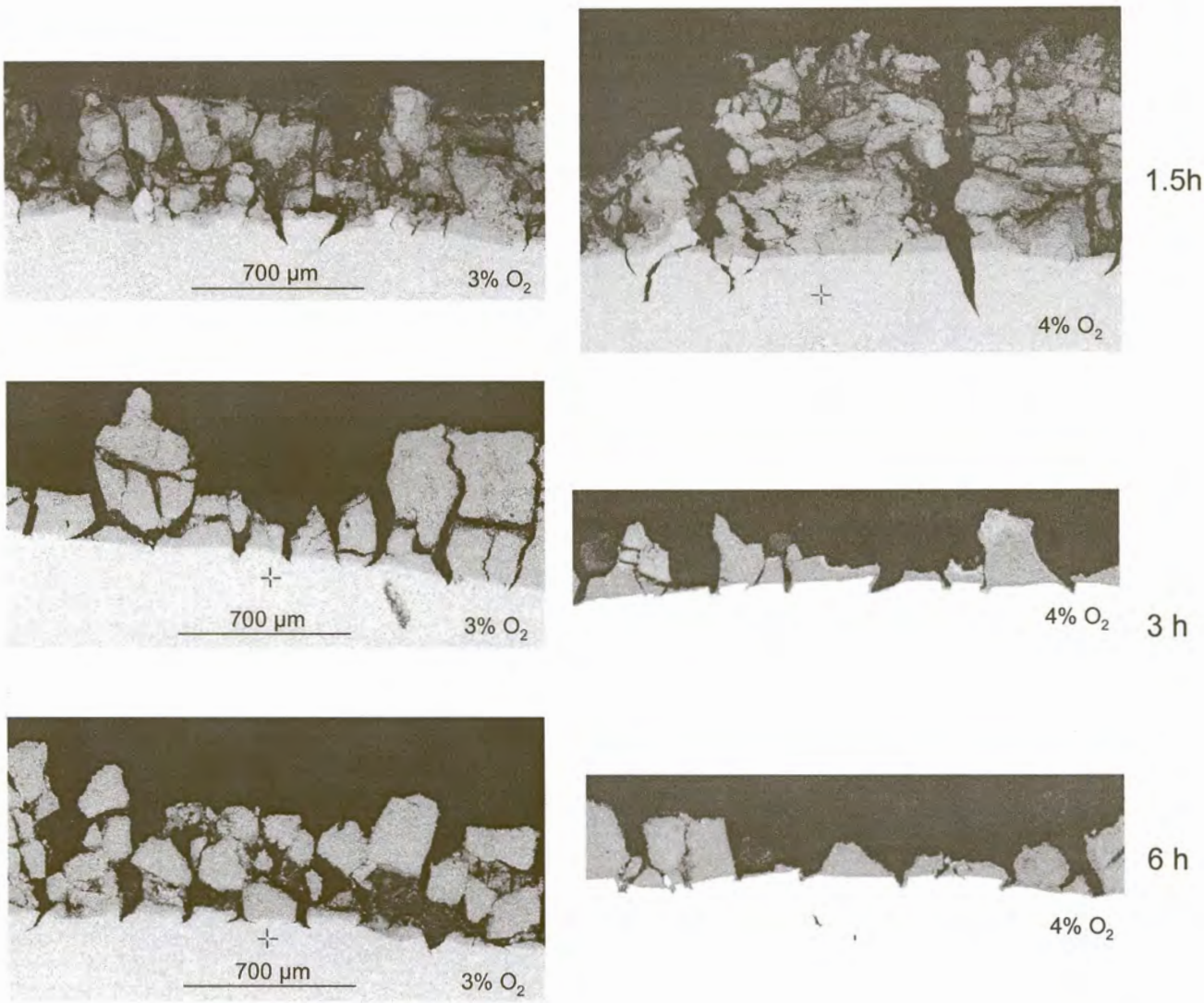

Figure 32 : Change in appearance of the residual scale, for type 304 stainless steel, after reheating at 1250 ^{0}C and mechanical descaling (scanning electron micrographs)

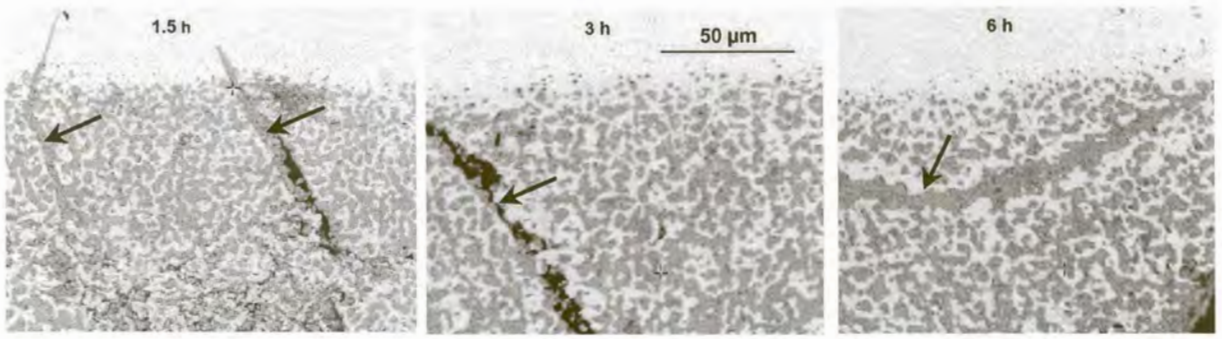

Figure 33 : Structure of scale close to scale-steel interface, for type 304 stainless steel reheated at 1250 ^{0}C in an atmosphere with 4% excess oxygen. Planes of metal-free chromite (arrowed) are evident. (The unoxidised substrate is shown in the upper parts of the three images.)

The correspondence between the austenite grain structure and the fracture paths is confirmed in figure 34, which shows cross-sectioned samples that had been etched (using electrolytic oxalic acid etch) to reveal the austenite grain structure. Cracks in the residual scale can be seen to correspond to grain boundaries in the underlying microstructure. This is also evident in figure 35 as well as appendix 7.

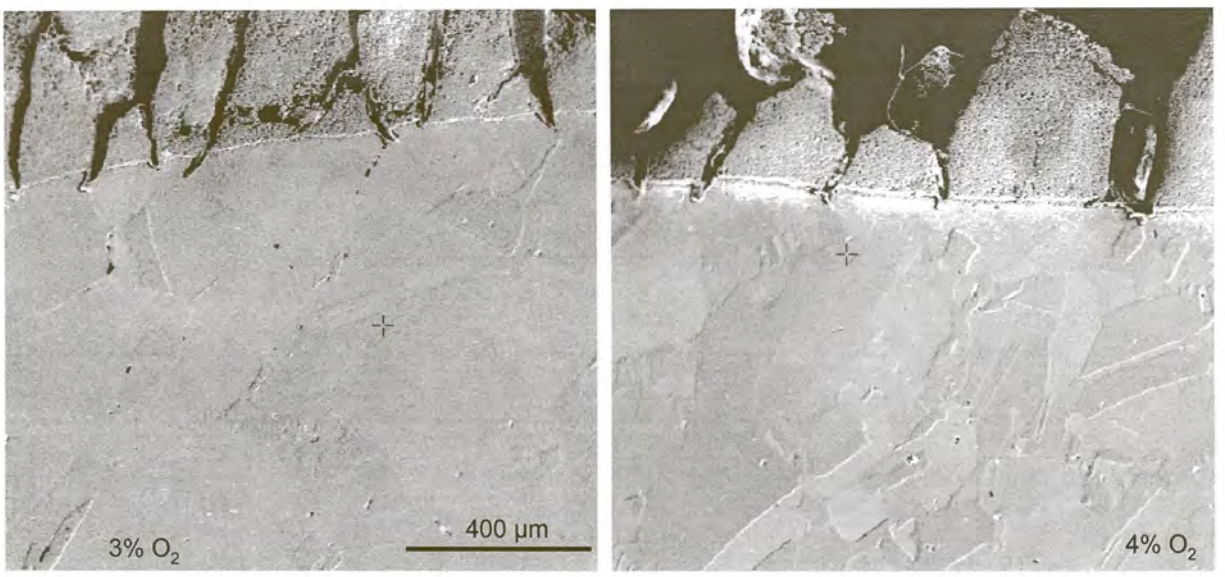

Figure 34 : Etched cross-sections of type 304 samples reheated at 1250 ^{0}C.

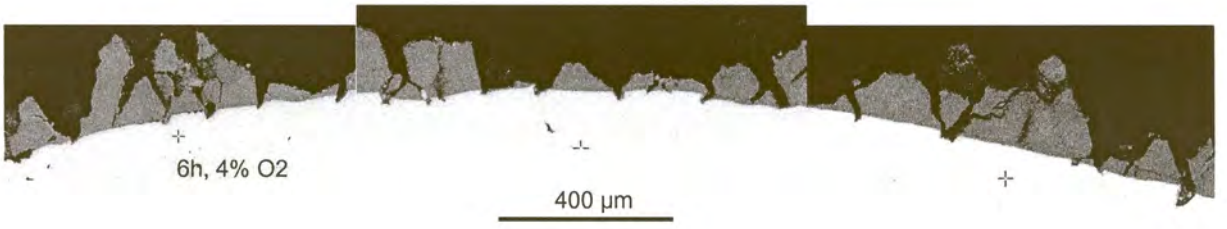

Figure 35 : Montage of descaled surface of type 304 sample (reheated at 1250 ^{0}C),

4.2.1.2 REHEATING TEMPERATURE : 1280 ^{O}C

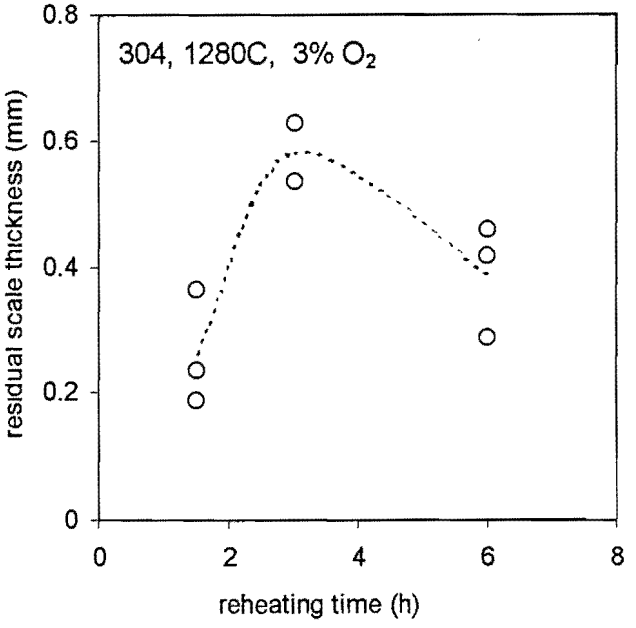

c)

Type 304, at 1280 ^{0}C, with 3% O_2

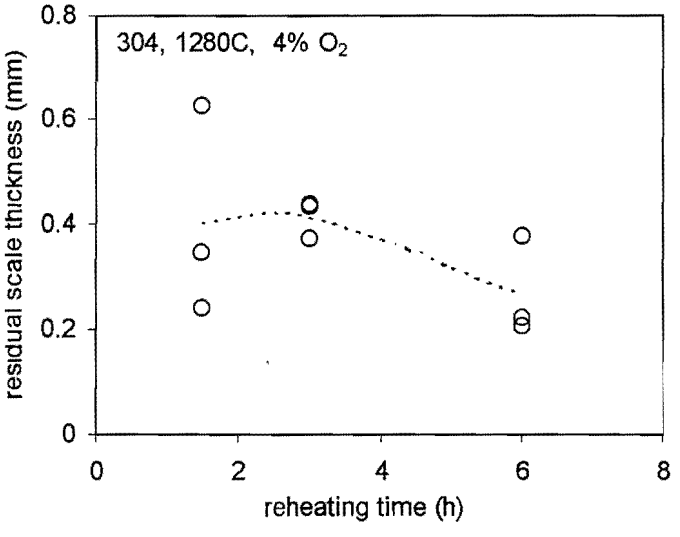

d)

Type 304, at 1280 ^{0}C, with 4% O_2

Figure 36 : Measured residual scale thickness for type 304 samples, reheated at 1280^{0}C, for varying times and with 3% and 4% oxygen in the furnace atmosphere

The graphs on the previous page (figure 36) show the measured residual scale thicknesses, for type 304 samples that were reheated at 1280 ^{0}C, for varying reheating times and with 3% and 4% oxygen in the furnace atmosphere. The residual scale somewhat decreased in thickness for higher excess oxygen and longer reheating. As was stated previously, this difference is caused by the way in which the type 304 samples descaled — by the formation of numerous cracks through the scale as is illustrated in figure 37 below.

On comparing the residual thicknesses at 1280 ^{0}C and at 1250 ^{0}C, it is evident that for both reheating temperatures, the residual scale again somewhat decreased in thickness for higher excess oxygen and longer reheating. However, slightly more residual scale is observed at the reheating temperature of 1280 ^{0}C (especially for 3% excess oxygen). As mentioned earlier, this can be explained by the way in which the samples descaled — by formation of cracks through the scale (or the lack of crack formation in this particular case, as seen on comparison of figures 32 and 37).

Etched cross-sections of samples, which were reheated at 1280 ^{0}C, are shown in figure 39. Cracks in the residual scale can be seen to correspond to grain boundaries in the underlying microstructure. The lack of cracks in this figure (resulting in the presence of slightly more residual scale at the reheating temperature of 1280 ^{0}C) is also evident on comparison with figure 34.

Small amounts of delta ferrite may serve to pin the austenite grain boundaries and so favour descaling – austenite crystals are produced during the transformation of primary delta ferrite crystals which are enriched with nickel and substantially depleted of chromium. Delta ferrite appears upon reheating at high temperatures, increasing in extent up to the melting point and from an Fe-Ni-Cr phase diagram, the formation of delta ferrite starts at a temperature of approximately 1250 ^{0}C (Folkhard, 1988).

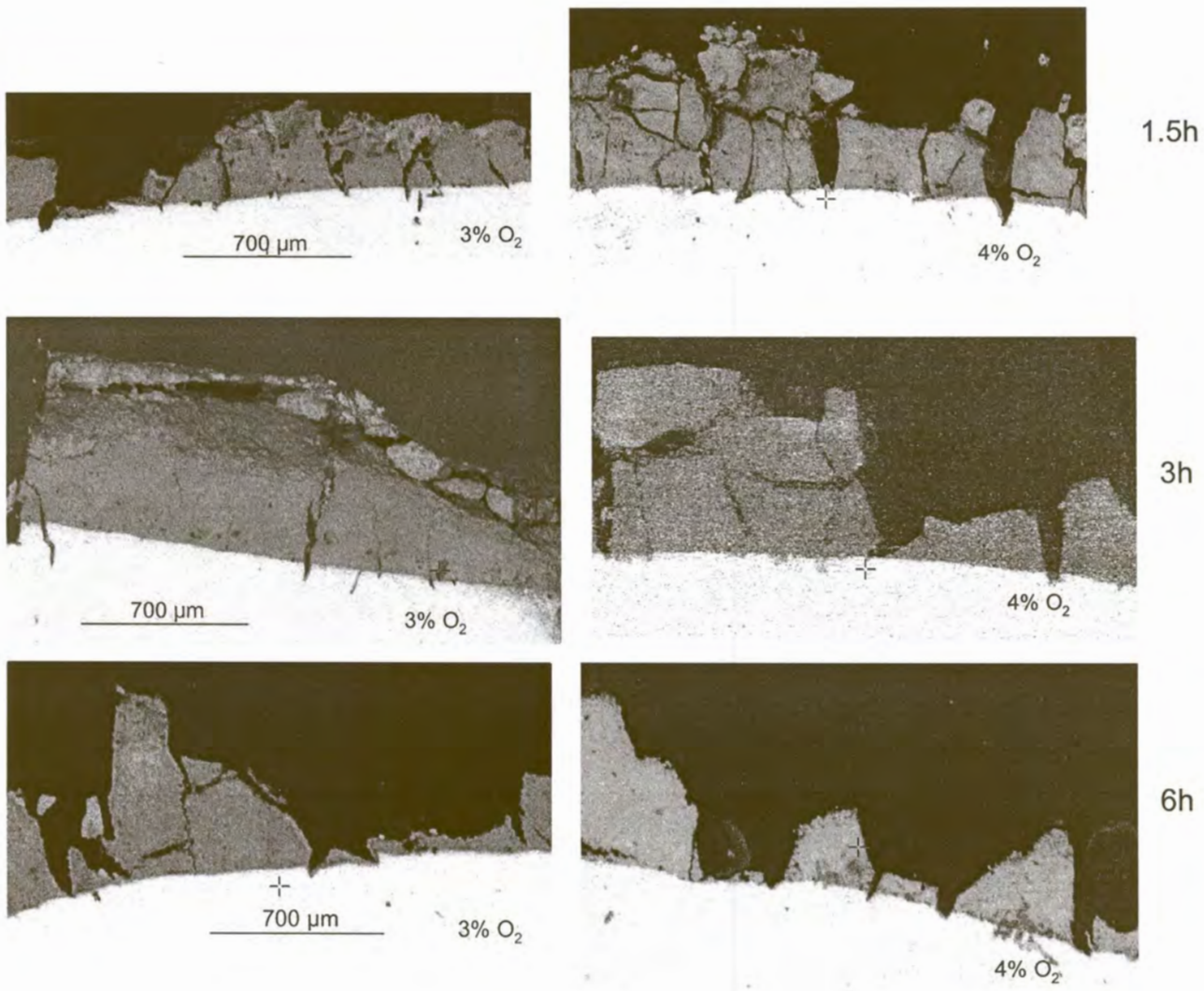

Figure 37 : Change in appearance of the residual scale, for type 304 stainless steel, after reheating at 1280 ^{0}C and mechanical descaling (scanning electron micrographs)

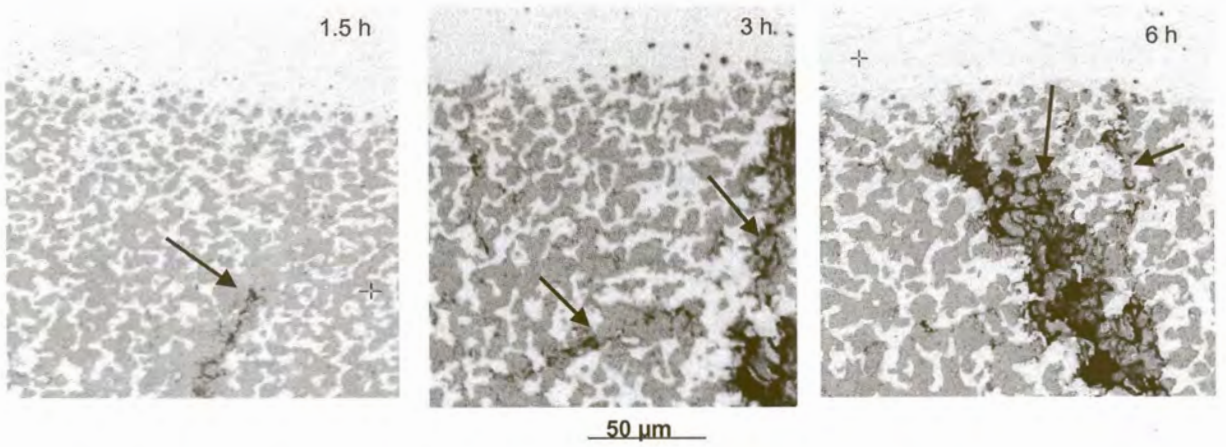

Figure 38 : Structure of scale close to scale-steel interface, for type 304 stainless steel reheated at 1280 ^{0}C in an atmosphere with 4% excess oxygen. Planes of metal-free chromite (arrowed) are evident. The unoxidised substrate is shown in the upper parts of the three images.

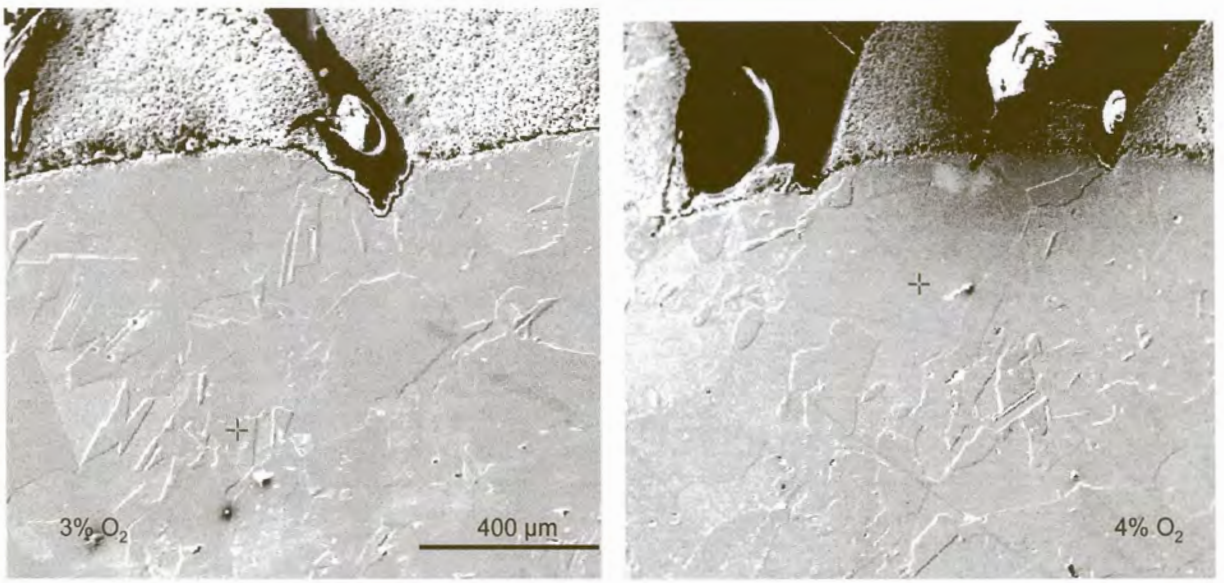

Figure 39 : Etched cross-sections of type 304 samples reheated at 1280 ^{0}C.

4.3. Comparison of type 304 and 412 stainless steel

The measured residual scale thicknesses for the two steel grades are shown in figures (24, 27, 31 and 36). These results show the behaviour of type 412 and type 304 to be quite different – while the former steel grade is quite sensitive to reheating time and excess oxygen; this is not the case for type 304. These differences (with time, atmosphere and steel grades) arise from differences in the structure of the scale. In figure 40, the appearance of the exterior surface of a descaled type 412 sample is presented.

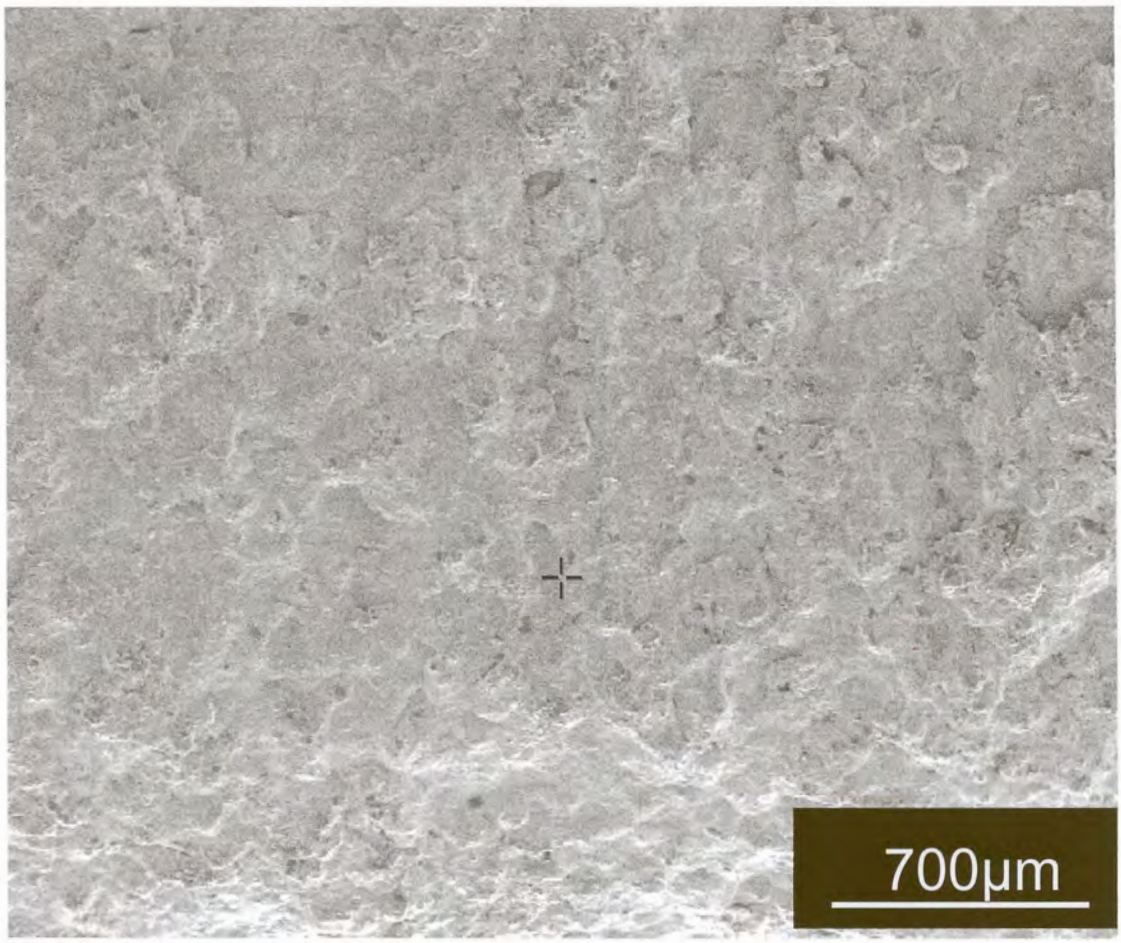

Figure 40 : Appearance of exterior surface of descaled type 412 sample

The correspondence between the austenite grain structure and the fracture paths for the type 304 stainless steel is evident in figure 41 below (as well as appendix 7), which shows the appearance of the as-descaled surface. The topography visible in this image is that of the residual scale attached to the stainless steel sample. The cracks through this residual scale can be seen to delineate a typical austenite grain structure.

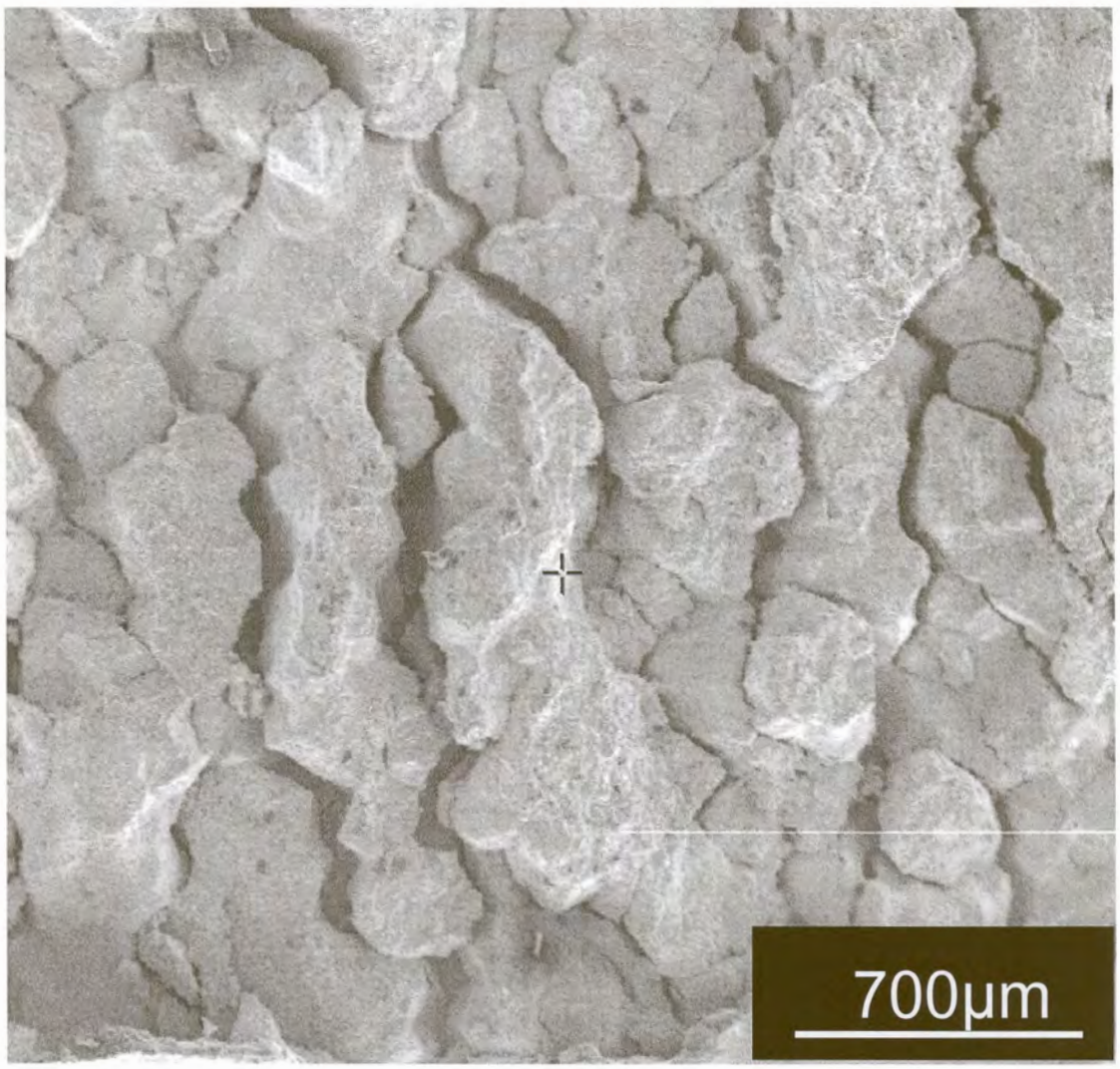

Figure 41 : Appearance of exterior surface of descaled type 304 sample, showing that the appearance of the cracked residual scale reflects the underlying austenite grain structure

5. Conclusion

The experimental results presented above indicate that the original hypothesis – that descaling is simply linked to the interfacial structure – does not fully explain the differences between steel grades and processing conditions. Descaling rather depends on the presence of metal-free fracture paths through the scale. In the case of type 412 stainless steel, these fracture paths lie at the outer edge of the entangled region (where the metallic fingers have been oxidized). The type 412 stainless steel showed greater sensitivity to reheating conditions and thus the amount of oxidation can be limited – by controlling the excess oxygen and the reheating time.

For type 304, the fracture paths followed the austenite grain boundaries (as a result of the formation of chromite layers at the grain boundaries, by internal oxidation). Control of the austenite grain structure is thus likely to have a strong effect on descaling for nickel-bearing stainless steel grades; small amounts of delta ferrite may serve to pin the austenite grain boundaries and so favour descaling (delta ferrite appears upon reheating at high temperatures, increasing in extent up to the melting point). Thus for the type 304, the effect of temperature on the residual scale thickness may probably be linked to the amount of delta ferrite that is formed and thus the austenite grain structure.

6. Recommendations

The difference in behaviour of the type 412 and 304 stainless steel suggests that different approaches favour descaling in industrial operations.

For type 412 (and by extension other nickel-free ferritic and martensitic grades) the amount of oxidation must be limited – by controlling the excess oxygen and the reheating time. For type 304, longer oxidation in more oxygen-rich atmospheres apparently favour descaling presumably because this allows more complete development of the chromite layers in the scale (the poor descaling of the samples reheated for only 1.5 hours likely originates from such an effect).

The grain structure of the as-cast slab also assumes an unexpected importance in descaling – if the extent of scale growth is such that the chill zone is fully oxidised, and the scale grows into the columnar zone, descaling is likely to be much poorer (and the extent of slab grinding is of relevant to this). This indirect effect may well account for much of the variability in descaling behaviour that is observed practically and perhaps this effect should be investigated as well. Thus samples from actual type 304 slabs (rather than rolled plate as used in this project) should be used to test the predicted effect of differences in grain structure on descaling. Actual scale samples from primary descaling operations could also be examined to test whether the predicted role of chromite layers is found in practice.